Jpn. J. Appl. Phys. Vol. 42 (2003) pp. 6590–6597
Part 1, No. 10, October 2003
©2003 The Japan Society of Applied Physics

Laser-Produced Plasma Experiments and Particle in Cell Simulation to Study Thrust Conversion Processes in a Laser Fusion Rocket

Konstantin V. VCHIVKOV*, Hideki NAKASHIMA, Yuri P. ZAKHAROV[1], Tomonori ESAKI, Toshihiko KAWANO and Takanobu MURANAKA[2]

Department of Advanced Energy Engineering Science, Kyushu University, 6-1 Kasuga-Kouen, Kasuga, Fukuoka 816-8580, Japan
[1]*Institute of Laser Physics (ILP), Novosibirsk 630090, Russia*
[2]*Institute of Laser Engineering, Osaka University, Suita, Osaka 565-0871, Japan*

(Received November 29, 2002; accepted June 9, 2003; published October 9, 2003)

An experiment is conducted to study the thrust conversion process of a laser fusion rocket (LFR) in a scaled-down manner. The temporal evolution of laser-produced plasma clouds (LPC) expanding in a dipole magnetic field is examined and the thrust conversion efficiency is estimated. For comparative purposes, numerical analyses of plasma behaviour in a dipole magnetic field are also performed using a three-dimensional (3D) hybrid particle-in-cell (PIC) code. An overall good agreement between the experimental and simulation data is found. It is also found that a thrust conversion efficiency as high as 60% is possible in the scaled-down model considered here. The experiments will be very useful in developing LFR designs and testing the basic features of the large-scale simulative LFR experiments proposed for the National Ignition Facility (NIF).
[DOI: 10.1143/JJAP.42.6590]

KEYWORDS: laser-produced plasma, dipole magnetic field, three-dimensional hybrid code, laser fusion rocket, thrust conversion

1. Introduction

A propulsion system driven by a laser-induced fusion called laser fusion rocket (LFR) is an innovative idea proposed by Hyde[1)] and it is an attractive candidate for future interplanetary missions since it could furnish both large specific impulse and power. A fusion reaction can release a large amount of energy and easily produce plasma of high temperature and density. The resulting plasma flow can be controlled by a properly designed applied magnetic field geometry, i.e., a magnetic thrust chamber. In the laser fusion rocket, the chamber is composed of a solenoidal superconducting coil.

The fusion reaction occurs by irradiation of a laser onto a fuel pellet and the resulting plasma expands isotropically at an early stage. The plasma is a good conductor, so when a magnetic field is applied, the plasma particles move around the magnetic field, i.e., Larmor motion starts. This circular motion induces diamagnetic currents, sweeping aside the field of the chamber. The compressed field, however, pushes against the plasma, and finally redirects the plasma to produce thrust. The chamber has advantage in that its thermalization with the wall structures of the thrust chamber can be avoided. Thus the laser fusion rocket could realize a very high exhaust velocity of plasma as compared with existing systems. This fact makes the laser fusion rocket a promising candidate for an interplanetary transport system.

Hyde[1)] designed a LFR for the first time and estimated its thrust efficiency using a two-dimensional magnetohydrodynamics (MHD) code. The efficiency in terms of momentum was reported to be 65%, where the thrust efficiency is defined as the ratio of $\Sigma m_i v_z$ to $\Sigma m_i |v_0|$, where m_i is the ion mass, v_z is the z-component of its velocity and $|v_0|$ is the absolute initial velocity. The sum Σ is carried over all the plasma particles.

A new spacecraft concept called Vehicle for Interplanetary Space Transport Applications (VISTA) was developed by Orth *et al.*[2,3)] This vehicle uses deuterium-tritium fusion. VISTA has a 6%-efficient excimer-laser driver operating at 1000 K with an output of 5 MJ, and uses pellets that allow energy gains from 200 up to perhaps 1500. Its effective specific impulse is about 17,000 s, with a thrust efficiency near 60%. When operating at a maximum pellet repetition rate of 30 Hz, VISTA's power system has a power-to-mass ratio near 20 W/g, a mass flow rate of 1.5 kg/s, a thrust of 2.4×10^5 N, and a jet power of 2.0×10^4 MW. These parameters allow a round-trip to Mars with a 100 metric ton (10^6 g) payload in about 100 days with a launch mass near 6000 metric tons.

VISTA's overall geometry is that of a 50° half-angle cone. This shape is required to avoid massive radioactive shielding and to keep fusion neutrons (and X-rays) from striking and heating vehicle surfaces. The 50° half angle maximizes the thrust efficiency, and is determined by selecting the optimum pellet firing position along the axis of the cone with respect to the plane of the magnetic coil, in a manner similar to that carried out by Hyde.[1)] The magnetic coil is located at the bottom of the spacecraft and the pellet is positioned at the apex of the cone, with two final laser focusing mirrors being used to irradiate the pellet.

Nagamine and Nakashima[4)] have investigated (a) whether Rayleigh–Taylor instability is significant for the plasma expansion in the LFR's magnetic thrust chamber and (b) how the efficiency for converting particle momentum into momentum along the rocket's thrust vector varies with certain parameters.

Zakharov *et al.*[5)] reviewed the physical background of LFR and its laboratory verification in simulation experiments with "usual" laser-produced plasma cloud (LPC) expanding in an axially symmetric dipole magnetic field. As a result of such a kind of "Impulse" experiment under dimensionless conditions close to the related project of the interplanetary spacecraft VISTA,[2,3)] a conversion efficiency of plasma momentum as high as 60% was obtained in this type of magnetic thrust chamber for the first time by various independent methods.

Nakashima *et al.*[6)] proposed to use ignition facilities such as NIF to examine the feasibility of the thrust chamber

*On leave from Institute of Laser Physics (ILP)

concept and to identify the plasma instability expected in the chamber since the facility could realize the same plasma conditions as supposed for the fusion rocket. However, before realizing such a real-scale demonstration, it is preferable to conduct a scaled-down experiment by which a direct comparison between numerical simulation and experimental efforts is possible. Such a comparison is important to understand the complicated physics of LFR. However, thus far, comparisons were made only for some early stages of the exploding plasma of the scaled-down model of LFR by Muranaka *et al.*[7] They studied plasma behavior in a dipole magnetic field using a 3D hybrid code. Results for the early stages of plasma evolution of a scaled-down model of LFR are compared with the experimental and MHD analytical data of Nikitin *et al.*[8] The dependence of plasma expansion on initial plasma energy and location are discussed by temporal evolutions of plasma position and magnetic field strength. Following the paper by Muranaka *et al.*,[7] the present paper is the second report that attempts to obtain a complete plasma evolution of the scaled-down model both experimentally and numerically.

Here we discuss the experimental work for examining the thrust conversion process of LFR in the scaled-down model. The expansion of LPC in the dipole field is studied under the conditions close to those in LFR magnetic thrust chamber.[5] In addition, we present the results of simulation studies using a 3D hybrid code to examine the plasma behavior in the chamber and to compare them with the experimental results for LPC.

The outline of the paper is as follows: In §2, we discuss our experimental parameters and the similarity criteria between our experiment and projects such as VISTA. The criteria are used to obtain the scaled-down model of LFR. Section 3 discusses the experimental setup. Section 4 presents the calculation model and method adopted here. The analysis of plasma behavior in the magnetic thrust chamber, the estimation of thrust conversion efficiency and the comparison of the experimental results with the simulation ones are presented in §5 along with their discussion. The conclusions are given in §6. Finally, in the Appendix, we specify how to obtain thrust efficiency by magnetic probe measurements.

2. Characteristics of Plasma Cloud Expansion

For the above-given problem, the necessity to apply sophisticated PIC-models to describe the plasma cloud behavior in LFR is determined by the conditions of the collisionless expansion of ions with a small but finite directed Larmor radius R_L on the characteristic scale R_b of cloud deceleration by magnetic field $\boldsymbol{B}_{d0}$ of the coil, where $R_L = m_i V_0/(Ze\boldsymbol{B}_{d0})$ and $R_b \approx (3\mu_0 E_0/(4\pi \boldsymbol{B}_{d0}^2))^{1/3}$, and m_i is the ion mass, V_0 the initial velocity, Z the charge rate, e the elementary electric charge, μ_0 the vacuum magnetic permeability and E_0 the kinetic energy. Retardation radius R_b is calculated under the condition that the kinetic energy density of all the plasma particles is equal to the density of the magnetic field energy. R_b accounts for the ideal characteristics of the retardation process, therefore some high-speed particles do not stop moving after R_b is reached.

As the result of Zakharov's experiment[9] on the interaction of LPC with a uniform magnetic field, the role of the general similarity criterion of problem $\varepsilon_b = R_L/R_b$ was established for the first time for exploding plasma clouds. The cloud interacts effectively with the field only under the condition of sufficient ion magnetization, i.e., $\varepsilon_b \leq 1$. In the opposite case, due to enhanced field penetration into plasma (with $\nu_{eff} \sim 0.3\omega_{ce}$ for electrons, where ν_{eff} is the electron turbulence frequency of the collisions and ω_{ce} is the electron cyclotron frequency), plasma cannot be decelerated by the field. One of the goals of the present "Impulse" experiment with LPC at the KI-1 facility was to check this critical ε_b for the case of a nonuniform dipolelike field typical of the LFR design[5] (see Table I).

Nikitin *et al.*[8] discussed the dynamics of the 3D expansion of a spherical cloud of rarefied plasma into a vacuum in the presence of a nonuniform external magnetic field of dipole structure, in the framework of ideal MHD approximation, and described how to determine the configuration and location of the plasma front as functions of time, and also how to determine the limits of its propagation, which are caused by the retardation effect. In addition, the authors of this paper defined another energetic criterion κ that characterizes the interaction between the expanding plasma and the dipole field and is given as

Table I. Comparison of various parameters.

Parameter		VISTA Project[2] for H_2-expellant	VISTA testing at NIF[4,6] (proposed)	KI-1,[5] experiment
Kinetic energy	E_0	500–1000 MJ	4 MJ	3–4 J
Exp. velocity	V_0	300 km/s	300 km/s	140 km/s
Plasma ions	$\langle m/z \rangle$	1 amu (H)	~10 amu	2.6 amu
Ejection point	R_0	11 m	1 m	15 cm
Magnetic field at R_0	B_{d0}	4 kG	9 kG	1 kG
Coil current	J_c	17 MA	4 MA	$\sim 10^5$ (A-Turn)
Coil radius	R_c	13 m	1 m	~5 cm
Magnetic moment	μ_d	10^{13} G·cm^3	10^{10} G·cm^3	2×10^6 G·cm^3
Ion magnetization criterion $\varepsilon_b = R_L/R_b$	ε_b	~0.001 ($\ll \varepsilon_{bc} \sim 1.3$–1.5)	0.02	≤ 1 ($< \varepsilon_{bc}$)
Energetic criterion $\kappa = 3E_0R_0^3/\mu_d^2$	κ	0.2–0.4 ($\leq \kappa_c = 0.4$)	~1	0.1 ($< \kappa_c$)

$$\kappa = \frac{E_0}{E_M} = \frac{12\pi E_0 R_0^3}{\mu_0 |\mu_d|^2},$$

where E_0 is the initial kinetic energy of ions, E_M the field energy integral of the dipole beyond the spherical radius $R_0(E_M = (\mu_0/4\pi)|\mu_d|^2/(3R_0^3))$, R_0 the distance from the magnetic coil to the explosion location and $|\mu_d|$ the magnetic moment magnitude. The critical criterion κ_c was found by Nikitin *et al.*[8] for a different plasma location. When κ is lower than κ_c, substantial plasma deceleration will occur in all directions from the explosion location ("quasi-capture" mode), while the plasma will not be captured by an ambient magnetic field when κ is greater than κ_c ("rupture" mode). (When the plasma is located at the axis, the critical value is $\kappa_c = 0.4$)

Table I compares the main parameters of the scaled-down experiment considered here (KI-1) and the parameters of projects such as VISTA. We can see that the criteria in the experiment satisfy the same conditions as those in the VISTA project. The value of the energetic criterion of the problem $\kappa \sim 0.1$–1 was close to the range of the VISTA project while the value of the general similarity criterion $\varepsilon_b = R_L/R_b \leq 1$ was sufficiently low to expect high diamagnetic properties of the plasma cloud.

3. Experimental Setup

To simulate the real processes of plasma momentum transfer in a dipolelike magnetic field and to determine thrust efficiency, Zakharov *et al.*[5] have conducted the "Impulse" experiment as shown in Fig. 1 at the KI-1 facility[10] on the release of quasi-spherical LPC, with an initial expansion velocity V_0 of ~140–200 km/s and a total kinetic energy E_0 of ~3–8 J at the axis of the quasi-stationary (~1 ms) dipole with a moment $\mu_d = (1–2) \times 10^6$ G·cm^3, and a stainless-still spherical shell of radius $R_d = 8$ cm. Plasma was generated at a background pressure of ~0.001 mTorr (~0.133 mPa) by means of CO_2-laser beams with a total energy of ~50–100 J irradiating the Nylon 6 $(C_6H_{11}ON)_n$ pellet target of 3–4 mm diameter (suspended by a thin metallic wire). The laser pulse of 70 ns-duration was sufficiently short to fulfill the condition of instantaneous, explosion-like energy release of LFR-thrust and the thickness of the dipole shell (a few mm) was larger than the penetration depth of the magnetic field disturbances b_θ caused by plasma moment μ_c. Therefore the shell could imitate the presence of a metallic surface of the Li-shield and Al-constructions surrounding the superconducting coil of VISTA.[2]

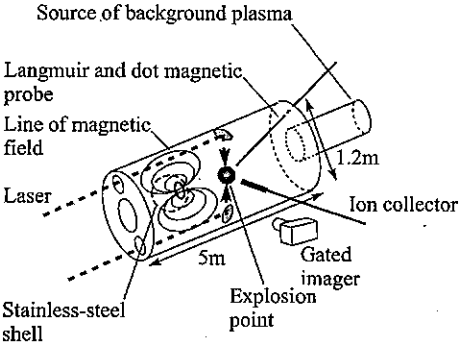

Fig. 1. Scheme of the experiment facility KI-1.

For diagnostic purposes in the "Impulse" experiment (Fig. 1) we have used a set of double Langmuir probes, shielded B-dot magnetic probes and the same probes at the dipole shell to determine its impulse via b_θ-measurements. All systems of diagnostics had resolutions higher than 1 cm and 30 ns, including a gated optical imager (GOI) that has registered the luminosity of the CIV-line (at 580 nm) excited by the charge-exchange of LPC ions in the presence of a specially added H_2-gas with a pressure of ~(0.1–0.2) mTorr. Such a method allow us not only to visualize but also to measure the spatial density distribution of the major C^{+4}-ion component of LPC (the other one is H^+).

4. Numerical Model

To calculate the plasma behavior under the dipole magnetic field we have developed a 3D hybrid PIC code based on the model given by Horowitz.[11] The hybrid code treats ions as individual particles and electrons as a fluid. This approach is valid when the system behavior is dominated by ion physics.

The equations controlling our system can be derived from Maxwell's equations and the equations of motion of particles. The basic equations of the model are as follows.

The electric field is computed from the momentum equation for an electron fluid

$$n_e m_e (dv_e/dt) = -en_e(E + v_e \times B) - \nabla P_e, \quad (1)$$

where m_e is the electron mass, n_e the electron density, e the elementary electric charge, v_e the electron velocity, E the electric field and B the total magnetic field. P_e is the electron pressure given by

$$P_e = n_e T_e, \quad (2)$$

where T_e is the electron temperature and is assumed to be uniform for simplicity.

The electrons are approximated as a massless fluid, so the left-hand side of eq. (1) becomes zero and

$$E = -v_e \times B - (1/en_e)\nabla P_e. \quad (3)$$

Ampere's law with Darwin approximation, which indicates that high-frequency electromagnetic waves do not exist, reduces to

$$\nabla \times B_p = \mu_0(J_e + J_i). \quad (4)$$

where B_p is the magnetic field generated by plasma current density. Substituting $-en_e v_e$ for J_e in Ampere's law, solving for v_e, and substituting v_e into eq. (3), we obtain

$$E = (1/\mu_0 Zen_i)(\nabla \times B_p) \times B - (1/Zen_i)J_i \times B - (T_e/en_i)\nabla n_i. \quad (5)$$

We assume quasi-neutrality and set the ion charge density equal to the electron charge density, i.e.,

$$Zn_i = n_e \quad (6)$$

in eq. (5), where Z is the charge state of the ion. Equation (5) includes the terms inversely proportional to the ion density n_i In a vacuum region, these terms must cause numerical infinity. We solve the Laplace equation to obtain the electric field in a vacuum region,

$$\nabla^2 E = 0. \quad (7)$$

Ion density n_i and current density J_i are calculated by the PIC method based on particle position x_i and velocity v_i which are obtained by integrating the equations of motion given as

$$dv_i/dt = (Ze/m_i)(E + v_i \times B), \quad (8)$$

$$dx_i/dt = v_i, \quad (9)$$

where m_i is the mass, Ze the charge, v_i the velocity and x_i the position of the ion.

The magnetic field is advanced by Faraday's law

$$\partial B/\partial t = \nabla \times E. \quad (10)$$

Cartesian coordinates (X, Y, Z) are adopted here. The time levels of the ion position and field quantities are defined at an integer time step, and the ion velocity and current density at a half-time step. The leap-frog method which is a time-centered difference scheme is adopted to solve the ion's equations of motion. Faraday's law is solved using the backward difference scheme in time. Field quantities, ion density and current density are spatially defined at the same grid points. The boundary condition adopted here for the field quantities is that the spatial differences of the normal components are set to be zero at the surface of the cylindrical calculation region.

The calculation model considered here is illustrated in Fig. 2 and is based on the experiment performed by Zakharov *et al.*[5]

The general calculation parameters used in the simulation are shown in Table II.

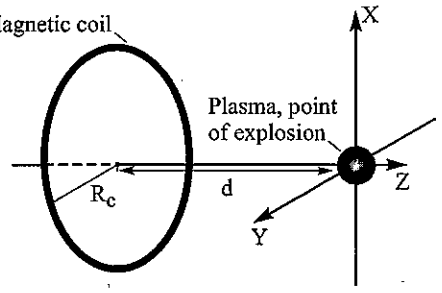

Fig. 2. Scheme of the calculation model.

Table II. Calculation parameters.

Coil radius (m)	0.05
Coil current (A)	2.52×10^5
Coil position along Z (m)	−0.15
Plasma coordinates (m)	(0,0,0)
Plasma radius (m)	0.021
Plasma energy (J)	3.5
Plasma mass (g)	0.6×10^{-6}
Atomic mass (AMU)	6.5
Atomic number	2.5
Magnetic moment μ_d (G·cm^3)	2×10^6
Initial magnetic field strength at the plasma (T)	0.1
Electron temperature (eV)	0
Initial max. velocity (km/s)	140
Time step Δt (μs)	0.00025
Calculation region (m)	$0.6 \times 0.6 \times 0.45$
Mesh size	$40 \times 40 \times 30$
Number of particles	100000

The initial distributions of the particle positions and velocities are assumed to be uniform. Here, the simulation starts from $t = 0.15$ μs to take account of the time elapsed for the plasma expansion to 2 cm in radius (we assume this, because until this time the plasma expands isotropically and there are no important changes in plasma shape). The initial plasma location is the same as in the experiment.

Here, we assume a single kind of plasma with a charge state Z of +2.5 and a mass of 6.5 amu by taking the average quantities of two ions H^+ and C^{4+} produced in the experiment.

5. Results and Discussion

In this section we present the simulation results along with the experimental results.

The numerical results for the time evolutions of particle position are shown in Figs. 3(a) and 3(b), where they are projected onto the XZ and XY planes, respectively. As is shown in these figures, the plasma shape is spherical at the initial stage and the plasma expands almost isotropically. Then the ions moving in the direction of the coil are reflected back by the magnetic field as explained in the Introduction, and the shape of the plasma changes to follow the dipole

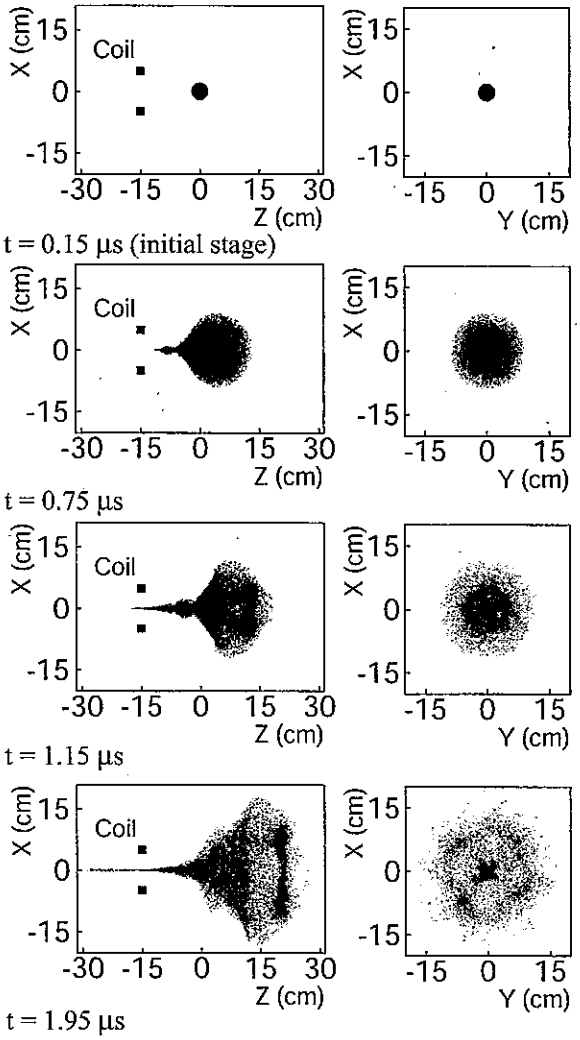

Fig. 3. Simulation results of particle positions projected onto the (a) XZ plane (left) and (b) XY plane (right).

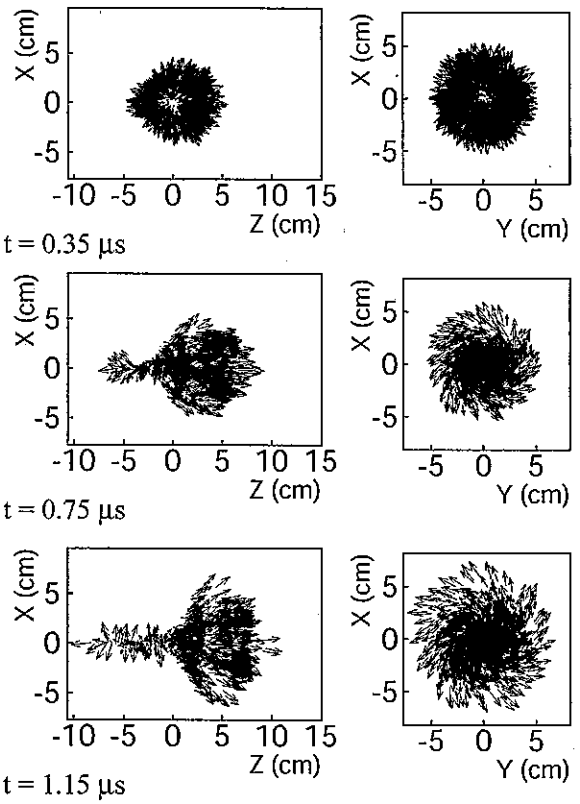

Fig. 4. Time evolution of velocity distributions at early stages projected onto the (a) *XZ* plane (left), and (b) *XY* plane at $Z \approx 5$ cm (right) (simulation results).

magnetic field line. On the other hand, as shown in Fig. 3(b), the shape of the plasma is symmetric at all the stages in the *XY* plane.

Figures 4(a) and 4(b) show the time evolutions of velocity distributions projected onto the *XZ* and *XY* planes at early stages. The velocity vectors are directed and displaced according to the magnetic lines of force. In Fig. 4(b), we can see the ion Larmor rotation of the plasma particles related to the diamagnetic exclusion of the magnetic field in the plasma.

We could not observe any clear evidence of plasma capture, although the parameter κ ($\kappa = 0.1$) was much less than the critical value of 0.4. Note that this critical value is obtained using the idealized MHD-Nikitin model. (Strictly speaking, the present experiment and calculation are not of the MHD case, because for the MHD model to be valid, the similarity criterion $\varepsilon_b = R_L/R_b$ should be much less than the critical value of 1.0; in the present experiment $\varepsilon_b \sim 1$.) Many approximations are adopted in the derivation of the critical value, hence the MHD-Nikitin model fails to reproduce the experimental results.

In contrast, our PIC code successfully simulates the plasma behavior as in Fig. 5, where the comparison between numerical and experimental results show good agreement. The experimental results are obtained using GOI for the particle position projected onto the XZ plane at a time of 0.75 μs. The simulation result is shown as a dashed line in the figure. As seen from the picture, the plasma shapes are almost identical between the simulation and experiment, although the asymmetrical expansion in the experiment made closer comparison difficult. The asymmetrical shape of plasma

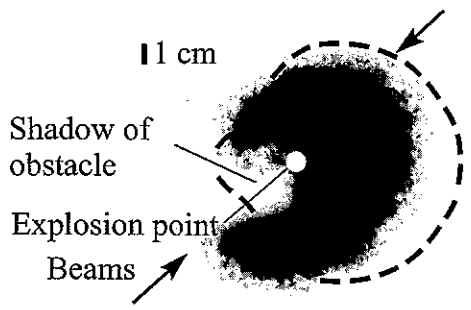

Fig. 5. Experimental results of the particle position projected onto the *XZ* plane at 0.75 μs. The dashed line is the particle position boundary of the simulation result.

expansion is related to the laser beam paths which corresponds to the preferable directions of plasma expansion (top right and bottom left). (We proposed using the Gekko XII facility in irradiating the target more uniformly[12]). Note also that the jet towards the magnet collides with the shell in Fig. 5, while in Fig. 3 the jet runs through the magnet because the shell enclosing the magnet is neglected in the simulation (see Fig. 2).

Figure 6 shows the time-integrated pictures of LPC: (a) experimental results and (b) simulation results. The experimental results were obtained using GOI. From the picture [Fig. 6(a)], we can see some features of secondary plasma luminosity at the ends of probe's supporting tubes. The simulation results were obtained by superimposition of plasma particle positions. The angle of LPC expansion is about 60° for both pictures.

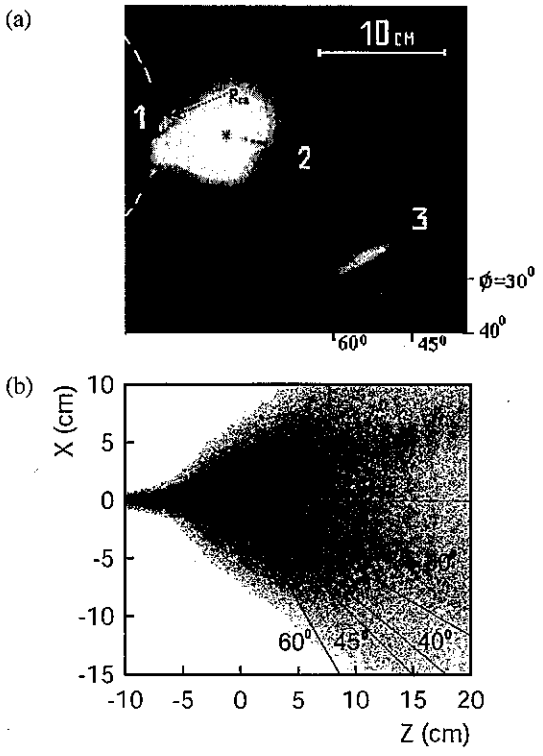

Fig. 6. Time-integrated picture of plasma cloud; (a) experimental results, 1 shell surface (with magnetic probe), 2 target supports (with a pellet on wire), 3 Langmuir probes, R_{ce} maximum effective radius of LPC diamagnetic cavity, ϕ angle of LPC expansion; (b) simulation results.

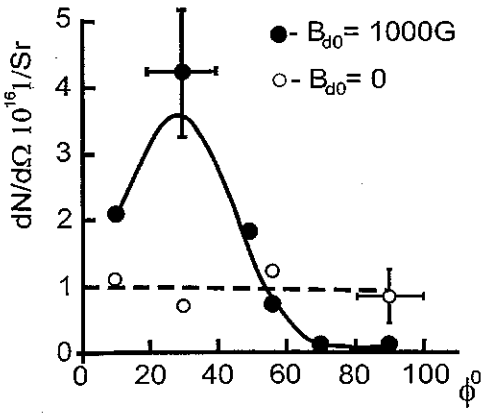

Fig. 7. Angular distribution of time-integrated plasma flow under conditions of LPC with $E_0 \sim 3$–4 J (experiment).

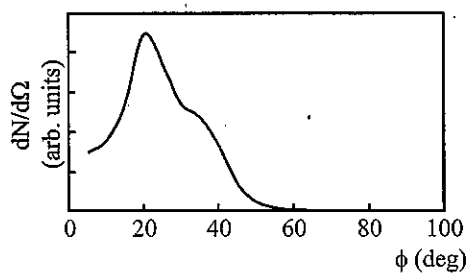

Fig. 8. Angular distribution of spatial-integrated plasma flow (simulation results).

Figure 7 shows the angular distribution of the plasma flow obtained by time integration of the data measured using double Langmuir probes in the experiment while Fig. 8 shows the distribution obtained by the simulation. Here, for comparison, we consider an arbitrary unit in Fig. 8, because we use discrete particles (each of which symbolized an action of many physical particles) in the simulation. For convenience, we used spatial integration instead of time integration, i.e., we registered the particles that locate beyond the radius of 25 cm at 3 μs, since the particles will not significantly change the trajectories around this time. We can see from these figures that the plasma flow is collimated by a magnetic field within an angle of ~60°. On the other hand when a magnetic field is absent ($B_{d0} = 0$), an isotropic plasma flow is obtained (see Fig. 7).

The experimental data on the magnetic field disturbances ΔB caused by the diamagnetic cavity of plasma are illustrated in Figs. 9(a) and 9(b). The signals on these figures are simple trace of B-dot magnetic probes. The signals are registered using an oscilloscope. The total errors of measurements are approximately (±) 7%, relative to any current signal amplitude. Figures 10 and 11 show the simulation data of magnetic field disturbances ΔB, which are obtained at various points of the simulation.

Curve 2 in Fig. 10 is similar to curve 2 in Fig. 9(a), however the value of the field displacement for the simulation data is more than that of the experimental data. On the other hand, the time of the field displacement for the simulation data is shorter than that for the experimental data.

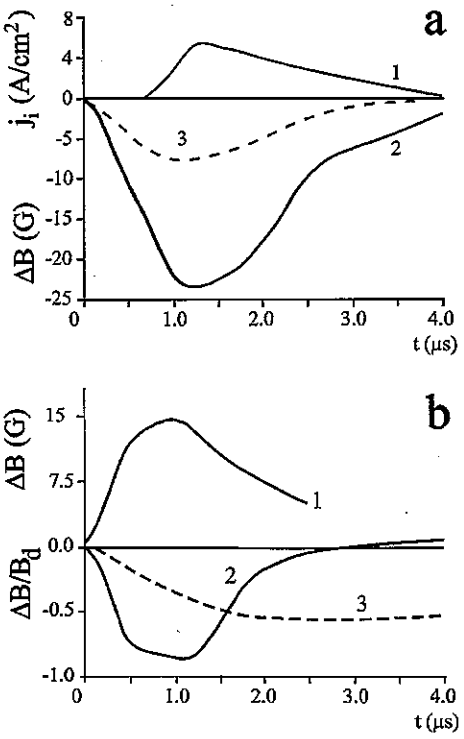

Fig. 9. The experimental data on magnetic field disturbances ΔB caused by the diamagnetic cavity of plasma obtained at various positions of magnetic probes. (a) 1 plasma flow ($R_p \approx 25$ cm, $\phi \sim 10°$), 2 ΔB ($R_p = 16$ cm, $\phi \approx 0°$), 3 ΔB ($R_p = 21$ cm, $\phi \approx 0°$); (b) 1 ΔB ($R_p = 14$ cm, $\phi \approx 90°$—outside of LPC), 2 ΔB ($R_p = 4.5$ cm, $\phi \approx 45°$), 3 ΔB ($R_p = 21$ cm, $\phi = 0°$).

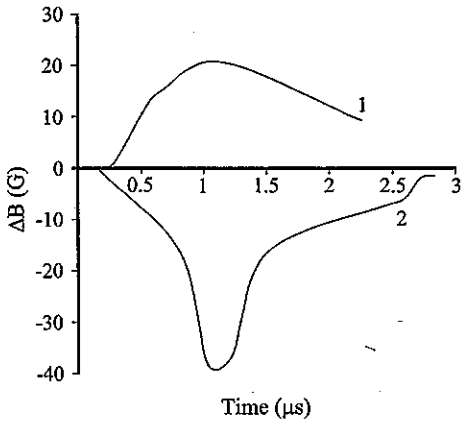

Fig. 10. Simulation data of magnetic field disturbances ΔB, 1 ($R_p = 14$ cm, $\phi \approx 90°$), [cf. curve 1 in Fig. 9(b)], 2 ($R_p = 16$ cm, $\phi \approx 0°$), [cf. curve 2 in Fig. 9(a)].

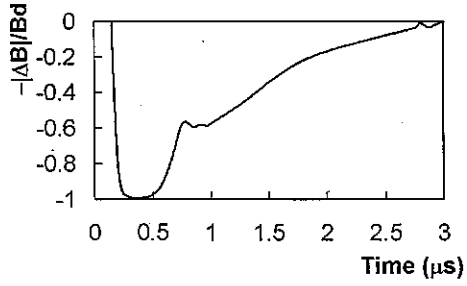

Fig. 11. Simulation data of magnetic field disturbances ΔB, normalized by the initial field B_d ($R_p = 4.5$ cm, $\phi \approx 45°$), [cf. curve 2 in Fig. 9(b)].

The same situation is observed for both the curve in Fig. 11 and curve 2 in Fig. 9(b). The probable reasons for the differences is that the number of discrete particles used is not sufficient in the simulation (we use 100000 in this calculation). In particular, the probe location of curve 2 in Figs. 10 and 9(a) is along the Z axis ($\phi \approx 0°$), so the solid angle around the probe is very small and very few particles come to this region, which results in ambiguity in the simulation. Curve 1 in Fig. 9(b) and the curve 1 in Fig. 10 show a rather good agreement.

The thrust efficiency η in terms of the momentum is calculated as follows:

$$\eta = \frac{\sum m_i v_z}{\sum m_i |v_0|},$$

where m_i is the ion mass, v_z the z-component of its velocity and $|v_0|$ the absolute initial velocity. The sum is carried over all the plasma particles. The results are shown in Fig. 12 as functions of time. η increases rapidly between 0.1 μs and 0.5 μs and then its value saturates at approximately 60% at 3.0 μs in Fig. 12. On the other hand, a value of about 60% was obtained from the experiment by measuring the impulse to the shell as shown in Fig. 13. The total measurement error of the thrust efficiency is approximately (±) 7% of its maximum value (60%). The measurement accuracy of thrust efficiency (through the impulse of the shell derived using the probe at its surface) is defined by the accuracy of the measurement of the magnetic field disturbances b_θ caused by plasma moment, dipole field B_ρ and initial plasma impulse (measured using the Langmuir probes). So the curve of experimental efficiency results from the traces of B-dot magnetic probes at the dipole shell, integrated as $b_\theta B_\rho/(\mu_0)$ over its surface and current time.[13] (See the Appendix for more detailed explanation.) All signals are registered using an oscilloscope with subsequent digitalization. A good agreement between the simulation and experimental results is obtained for the thrust efficiency.

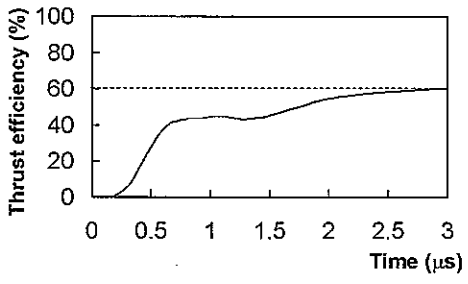

Fig. 12. Time evolution of thrust efficiency (simulation result).

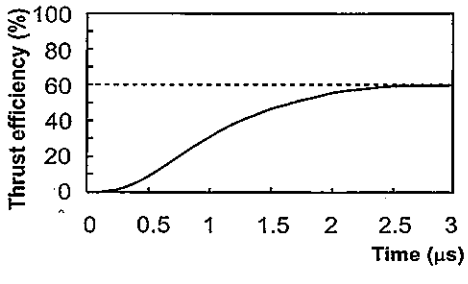

Fig. 13. Time evolution of thrust efficiency (experimental result).

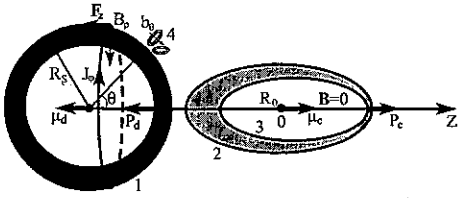

Fig. A·1. General scheme of "Impulse" experiment.

6. Conclusion

The LFR is a promising candidate for an interplanetary transport system. An experiment was conducted to study the thrust conversion process of LFR in a scaled-down manner. The temporal evolution of LPC expansion in a dipole magnetic field was examined and thrust conversion efficiency was estimated. For comparative purposes, we have carried out numerical analyses on plasma behaviors in the dipole magnetic field using a 3D hybrid PIC code. An overall good agreement between the experimental data and the numerical analyses was found. It was then concluded that a thrust conversion efficiency as high as 60% is possible in the scaled-down model considered here. It was also found that the experiments will be very useful in developing LFR designs and testing the basic features of the large-scale simulative LFR experiments proposed for NIF. For future engineering applications, these results will be useful in designing an optimal configuration of the magnetic thrust chamber for LFRs.

Appendix

The direct determination of dipole momentum P_d via magnetic field disturbances b_θ and dipole field B_ρ was described by Zakharov *et al.*[13] The determination of P_d is based on the new method of magnetic probe measurements of the volume force $F_z^p \propto J_\varphi B_\rho$ arising in the surface S of the shell housing of dipole μ_d (with its own field B_ρ at S, see Fig. A·1) when the plasma diamagnetic cavity appears, and the skin current J_φ should be generated to exclude from the conductive housing the magnetic field b_θ (of plasma moment μ_c). More strictly speaking, this b_θ field is the sum of the field of plasma moment μ_c and the field of its "image" inside the shell, with the moment $\mu_{ci} = \gamma^3 \mu_c$ shifted from the shell center toward μ_c to the distance γR_S (where the additional similarity criterion of the problem of the "shielded dipole" is $\gamma = R_S/R_0$, R_S being the dipole shell radius and R_0 the point of injection). In the case of very thin skin-layer of J_φ, the volume integration of its ponderomotive force $f_z^p = j_\varphi B_\rho$ could be replaced (using Maxwell tensor) by the surface one and a very useful relation for measuring the dipole impulse could be obtained as follows:

$$P_d = (1/\mu_0) \int dt \int b_\theta B_\rho dS \equiv \int F_z^p dt.$$

1) R. A. Hyde: UCRL-88857 Lawrence Berkeley Laboratory, 1983.
2) C. D. Orth, G. Klein, J. Sercel, N. Hoffman, K. Murray and F. Chang-Diaz: AIAA-87-1904, 1987.
3) C. D. Orth, G. Klein, J. Sercel, N. Hoffman, K. Murray and F. Chang-

Diaz: UCRL-96676, 1987.
4) Y. Nagamine and H. Nakashima: Fusion Technol. **35** (1999) 62.
5) Y. P. Zakharov, A. V. Melekhov, V. G. Posukh and I. F. Shaikhislamov: Current Trends in International Fusion Research—Abstr. 4th Symp., 2001, p. 31.
6) H. Nakashima, Y. Nagamine, N. Yoshimi, Y. P. Zakharov and A. G. Ponomarenko: Fusion Eng. Design **44** (1999) 359.
7) T. Muranaka, H. Uchimura, H. Nakashima, Y. P. Zakharov, S. A. Nikitin and A. G. Ponomarenko: Jpn. J. Appl. Phys. **40** (2001) 824.
8) S. A. Nikitin and A. G. Ponomarenko: J. Appl. Mech. Tech. Phys. **34** (1993) 745.
9) Y. P. Zakharov, A. M. Orishich, A. G. Ponomarenko and V. G. Posukh: Sov. J. Plasma Phys. **12** (1986) 674.
10) Y. P. Zakharov, V. M. Antonov and A. V. Melekhov: AIP Conf. Proc. 369, 1996, p. 357.
11) J. E. Horowitz, D. E. Shumaker and D. V. Anderson: J. Comput. Phys. **84** (1989) 279.
12) H. Nakashima: Presented at 4th US-Japan Workshop on Laser-Driven Inertial Fusion Energy Technology, Osaka University, 2003.
13) Y. P. Zakharov and H. Nakashima: Proc. 9 Int. Conf. Emerging Nuclear Energy Systems, Dan Knassim Ltd., Ramat Gan, Israel 1, 1998, p. 384.